Complex Oscillatory Yielding of Model Hard-Sphere Glasses

N. Koumakis,[1] J. F. Brady,[2] and G. Petekidis[1,*]

[1]FORTH/IESL and Department of Materials Science and Technology, University of Crete, 71110 Heraklion, Greece
[2]Division of Chemistry and Chemical Engineering, California Institute of Technology, Pasadena, California 91125, USA

(Received 1 February 2013; published 23 April 2013)

The yielding behavior of hard sphere glasses under large-amplitude oscillatory shear has been studied by probing the interplay of Brownian motion and shear-induced diffusion at varying oscillation frequencies. Stress, structure and dynamics are followed by experimental rheology and Browian dynamics simulations. Brownian-motion-assisted cage escape dominates at low frequencies while escape through shear-induced collisions at high ones, both related with a yielding peak in G''. At intermediate frequencies a novel, for hard sphere glasses, double peak in G'' is revealed reflecting both mechanisms. At high frequencies and strain amplitudes a persistent structural anisotropy causes a stress drop within the cycle after strain reversal, while higher stress harmonics are minimized at certain strain amplitudes indicating an apparent harmonic response.

DOI: 10.1103/PhysRevLett.110.178301 PACS numbers: 83.80.Hj, 83.10.Mj

Hard sphere (HS) colloids have been used as model systems to study a plethora of fundamental condensed matter problems such as the interplay between equilibrium phases (crystals and liquids) and nonergodic states (glasses or gels), and their behavior under external fields such as shear [1,2]. A major goal is to develop an understanding that will enable tailoring of the mechanical and flow properties based on the structure and dynamics at the particle level. HSs form metastable glasses above a volume fraction of about $\varphi_g \sim 0.59$ where crystallization and long-time diffusion are suppressed [3,4]. Such states exhibit solidlike behavior at low stresses or strains and shear-melting (yielding) above a yield stress or strain [5]. This phenomenon is investigated more effectively with a combination of rheological and optical or scattering techniques that may unravel the link between microstructure, dynamics, and mechanical properties in steady [6,7] or oscillatory shear [8,9]. Such studies have shown that particle cages are deformed under shear and particles move irreversibly when a critical strain is exceeded, leading to flow.

Experimentally, large-amplitude oscillatory shear tests are widely used to monitor yielding due to their simplicity and relation with linear elastic and viscous moduli, G' and G''. However, their interpretation in the nonlinear regime becomes complex due to stress distortion introducing higher harmonics [10]. In a wide range of systems (emulsions, polymers, and colloids) a generic peak in G_1'' (viscous modulus of the fundamental frequency) is observed representing an increased energy dissipation near the yield strain, γ_y, where $G_1' = G_1''$, beyond which the sample flows [9,11]. On the theory side, mode coupling theory (MCT) [12] as well as the semi-phenomenological soft glassy rheology [13] are able to capture some aspects of large-amplitude oscillatory shear (LAOS) such as the peak of G_1''. Nevertheless, the underlying mechanisms relating stress with shear induced structure such as cage deformation, breaking, and reformation, as well as particle displacements, are poorly understood, and the frequency dependence is largely unexplored.

LAOS experiments are expected to provide valuable information on the interplay of Brownian motion and shear during yielding of HS glasses. Along this line, light scattering-echo experiments probing the average particle displacements under oscillatory shear [8,9] revealed a transition to irreversibility beyond a critical strain amplitude [8,9]. This can be viewed as the analogue of the shear induced irreversibility observed in concentrated non-Brownian particles [14], since, at rest, diffusion is absent at all length scales in non-Brownian particles, while in colloidal glasses only the out-of-cage diffusion is frozen. While experiments combining rheometry with scattering or microscopy are rather demanding [8,15–18], computer simulations can provide an alternative route.

Here, we use a combination of oscillatory shear rheometry and Brownian dynamics (BD) simulations to investigate the links between structure and particle dynamics with the nonlinear rheological response of HS glasses in a wide range of frequencies, ω, nondimensionalized by Peclet number $\mathrm{Pe}_\omega^0 = \omega\tau_B$, with $\tau_B = R^2/D_0$, R the radius and D_0 the free diffusion coefficient, or Pe_ω if the short-time self diffusion coefficient $D_s(\varphi)$ is used. At low Pe_ω^0 yielding is related to Brownian-assisted irreversible particle motion manifested in a dynamic strain sweep (DSS) with the peak of G_1''. However, at the largely unexplored regime of high Pe_ω^0, we detect collision-dominated yielding and, within the oscillation period, a strongly anisotropic structure causing a reduced stress beyond strain reversal (memory of structure due to lack of Brownian relaxation). At intermediate Pe_ω^0, the sample is affected by both mechanisms as manifested by a novel, for HS glasses, double peak in G_1''.

We used model sterically stabilized poly(methyl methacrylate) nearly hard-sphere particles with two radii,

$R = 358$ and 130 nm (polydispersity 10%–12%) suspended in an octadecene and octadecene-bromonapthalene mixture respectively, in order to expand the Pe_ω range. We prepared different volume fractions, φ, by diluting a random close packed batch with the exact φ, then adjusted by matching G_1' of the two systems in agreement with Ref. [19]. Experiments were performed on an ARES strain controlled rheometer (with 25 mm diameter, 0.01 rad angle cone plate) and a solvent trap to eliminate evaporation. In BD simulations (described in the Supplemental Material [20]), HS interactions were implemented through the potential free algorithm [21]. Oscillatory shear was applied with periodic boundary conditions using typically 5405 particles with 10% polydispersity to avoid crystallization.

In Fig. 1, we show DSS tests performed at low and high Pe_ω, together with the evolution of the normalized intensity of all higher stress harmonics, $I_{\mathrm{all}}/I_1 = \sum I_i/I_1$, $(i = 2n+1, \quad n \geq 1)$, as well as Lissajous curves (intracycle stress versus strain) for representative strain amplitudes, γ_0. The low $\mathrm{Pe}_\omega (= 0.5)$ data [Fig. 1(a)] exhibit the typical DSS response with a G_1'' peak around γ_y (at $G_1' = G_1''$) similar to previous studies [11,19,22]. The nonlinear response is accompanied by progressively larger intracycle nonlinearities as indicated both by the Lissajous curves and the increasing I_{all}/I_1 as expected [10,19]. The latter increases beyond yielding and reaches almost 30% at high γ_0 as found previously [19]. Moreover, the Lissajous plots show a transition from a linear viscoelastic behavior (elliptical shape) at low γ_0, to a parallelogram pattern indicative of an intracycle sequence of elastic-plastic response at $\gamma_0 > \gamma_y$ [10,19].

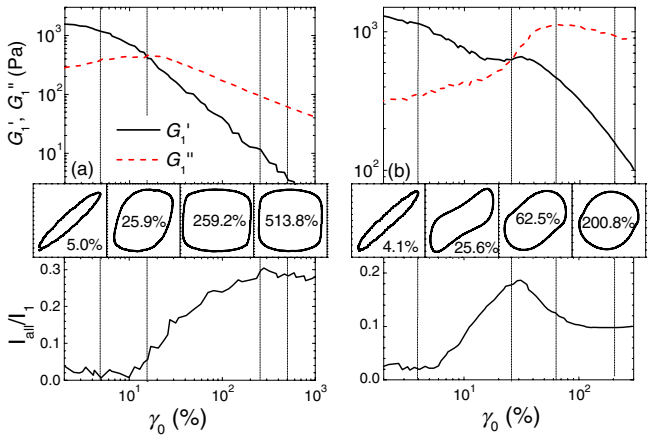

FIG. 1 (color online). Top: Dynamic strain sweeps for (a) $R = 130$ nm, $\varphi = 0.60$ at $\omega = 1$ rad/s $(\mathrm{Pe}_\omega^0 = 0.04, \mathrm{Pe}_\omega = 0.5)$ and (b) $R = 358$ nm, $\varphi = 0.60$ at $\omega = 1$ rad/s $(\mathrm{Pe}_\omega^0 = 0.9, \mathrm{Pe}_\omega = 11.2)$, with the 1st harmonic of the elastic G_1' and viscous G_1'' modulus as a function of strain amplitude. Middle: Representative Lissajous plots are shown in different strain amplitudes as indicated. Bottom: Normalized total intensity of the higher harmonics of the stress, I_{all}/I_1.

At high Pe_ω, achieved with large particles $(R = 358$ nm) at $\omega = 1$ rad/s $(\mathrm{Pe}_\omega = 11.2)$, the response is qualitatively different [Fig. 1(b)]. First, the peak of G_1'' shifts to higher γ_0, beyond γ_y. Second, I_{all}/I_1 (and individual I_{2n+1}/I_1) exhibits a nonmonotonic behavior showing a first maximum around γ_y and subsequently decreases substantially well inside the nonlinear regime. Hence, the sample exhibits a more harmonic stress response (anharmonicity is lowered) even though under nonlinear LAOS.

We further explore the Pe_ω dependence by changing ω while keeping γ_0 constant. In Fig. 2(a), experiments with varying ω (at $\gamma_0 = 100\%$) reveal the transition from the low-Pe_ω rectangular shaped Lissajous curves reflecting a sequence of elastic and plastic responses, to the high-Pe_ω regime with a characteristic *ellipsoid with a double concave distortion* caused by reduced stress in the quadrants II and IV after strain reversal. The intensity of the 3rd harmonic at 100% (above γ_y) exhibits a minimum with ω in experiments, $\varphi = 0.62$, and BD, $\varphi = 0.60$, [Fig. 2(c)]; note that the position of minimum is φ and γ_0 dependent. While in both Pe_ω regimes the stress response is highly anharmonic, with significant I_3/I_1, during the transition, the Lissajous curves [Fig. 2(a)] acquire an ellipsoid shape involving almost zero higher harmonic contributions. BD simulations showing identical rheological response [Fig. 2(b)] with experiments are able to provide valuable structural information revealing the underlying mechanism of such stress reduction. In Fig. 2(d), we plot the 2D projection of the pair correlation function (calculated in a

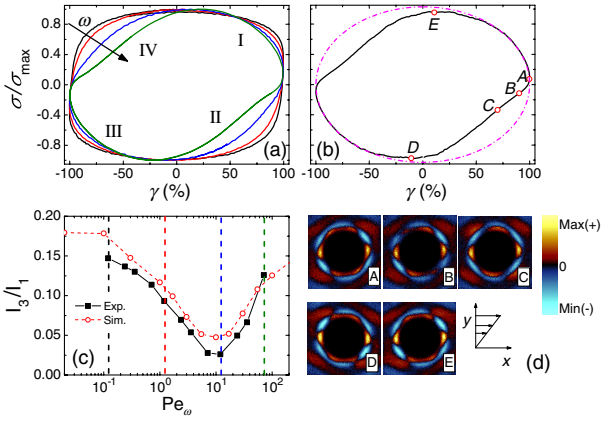

FIG. 2 (color online). Lissajous plots at 100% strain amplitude (a) for experiments at different Pe_ω denoted by the dashed lines in (c) with the 4 quadrants of the oscillatory cycle indicated and (b) BD simulations at $\mathrm{Pe}_\omega = 100$. The dashed line in (b) indicates a viscous harmonic stress strain response (see also Supplemental Material [20]). (c) Pe_ω dependence of the 3rd harmonic at 100%, for experiments at $\varphi = 0.62$ $(R = 358$ nm) and BD simulations at $\varphi = 0.60$. (d) 2D projections in the velocity-gradient (xy) plane of the difference of $g_{xy}(r)$ under shear from that at rest from BD simulations at indicated points within the cycle, points $A - E$ in (b).

thin slice of $\pm 0.7R$) in the velocity-gradient (xy) direction, $g_{xy}(r)$, at specific points inside the oscillation cycle for $\mathrm{Pe}_\omega = 100$, similar to findings under steady shear [7]. Contrary to what we find at low Pe_ω (Supplemental Material [20]), here the structure is highly anisotropic at the point of maximum strain [zero shear rate; point A in Fig. 2(b)]. Moreover, such anisotropy is persistent during a large part of the successive quadrant where the shear has been reversed (points B and C). Such an anisotropic cage, created during high Pe_ω shear in one direction, allows flow with less stress (due to fewer particle collisions) when shear is reversed. Thus, in quadrants II and IV the stress is reduced if compared to a fully harmonic viscous response corresponding to the flowing anisotropic structure of quadrants I and III [dashed-dotted line in Fig. 2(b)]. Only beyond zero strain (points D and E), is the structure reversed and the stress comes back to the maximum values within the period (see Supplemental Material [20]). Such a response is absent at low Pe_ω since Brownian motion relaxes shear-induced structural anisotropy more efficiently, and the stress response is similar in all quadrants.

The data presented above verify the existence of the two Pe_ω regimes: the low Pe_ω one, conventionally studied up to now, where Brownian motion is dominant, and the high Pe_ω where shear-induced particle collisions introduce novel LAOS features related to the persistent structural anisotropy and the consequent reduced stress after strain reversal. The transition from Brownian activated yielding, where particles under shear escape their cages assisted by thermal motion, to collision-induced cage breaking at high frequencies is linked to pronounced irreversible particle rearrangements and decreasing γ_y at low frequencies [8,9].

We further investigated HS glasses at higher φ and frequencies corresponding to an intermediate (φ dependent) Pe_ω regime. Experimental DSS, Lissajous plots, and I_{all}/I_1, shown in Fig. 3 as a function of γ_0 for $\varphi = 0.639$, reveal an even richer mechanical response at $\mathrm{Pe}^0_\omega = 0.4$ ($\mathrm{Pe}_\omega = 8$). A main observation here is the unambiguous detection of two peaks in G_1'' detected for the first time in HS glasses. Such a feature was so far observed only in attractive glasses and gels indicating a two-step yielding due to two length scales present in attractive systems, i.e., the interparticle bond and the cage or cluster size [22,23]. However, the double G_1'' peak seen here must be of a different nature since a second length scale is absent, and moreover, the phenomenon is only observed in a narrow range of Pe_ω. The first peak of G_1'' is identified with the one observed at low Pe_ω by a direct comparison of the two DSSs ($\mathrm{Pe}^0_\omega = 0.04$ and 0.4) shown in Fig. 3(a). The two peaks signify the maximum in energy dissipation during the two yielding mechanisms at low and high Pe^0_ω, attributed to cage breaking via shear-assisted activated hopping and through particle collisions, respectively. The Lissajous figures and higher harmonics

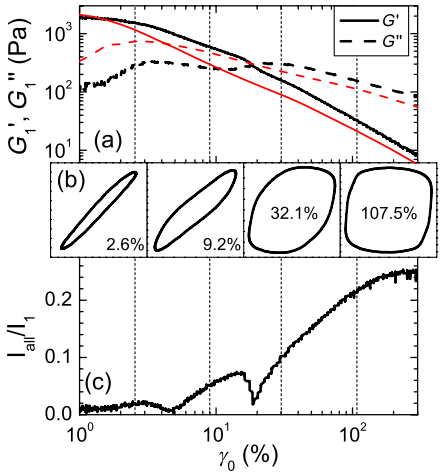

FIG. 3 (color online). (a) Dynamic strain sweeps with $R = 130$ nm particles at $\varphi = 0.639$ and an intermediate ($\omega = 10$ rad/s, $\mathrm{Pe}^0_\omega = 0.4$, $\mathrm{Pe}_\omega = 8$ thick black lines) and low ($\omega = 1$ rad/s, $\mathrm{Pe}^0_\omega = 0.04$, $\mathrm{Pe}_\omega = 0.8$ thin red lines) frequency regime. (b) Indicative Lissajous plots for $\mathrm{Pe}_\omega = 8$ at different strain amplitudes and (c) normalized total intensity of higher harmonics I_{all}/I_1, versus strain amplitude for $\mathrm{Pe}_\omega = 8$.

reveal a transition from the low γ_0 linear response to a viscoplastic flow at high γ_0 passing through two states with an apparent harmonic response as indicated by the two minima of I_{all}/I_1. At these strain amplitudes the Lissajous curves acquire a nearly ellipsoidal shape due to the compensation of the structural phenomena during the transition from low to high Pe_ω [as in Fig. 2(c)]. Note that for this sample ($R = 130$ nm, $\varphi = 0.639$) the high Pe_ω [Fig. 1(b)] was not within the experimental window.

Figure 4(a) shows G_1' and G_1'' from BD LAOS tests for $\varphi = 0.60$ at different Pe_ω. The dependence of G_1' and G_1'' at high γ_0 ($> \gamma_y$) follows a power law decrease $G_1'(G_1'') \propto \gamma_0^{\nu'}(\gamma_0^{\nu''})$ as detected experimentally [11,19]. While Maxwell-type models give $\nu' = 2\nu'' = -2$ and MCT (around the glass transition) predicts lower values, but similar ν'/ν'' ratio [12,24] experiments in HS glasses show deviations from such simple dependency [19]. In agreement with experiments (Fig. 1), BD simulations give Pe_ω dependent exponents [Fig. 4(a)] with ν'' approaching -1 and 0 at low and high Pe_ω, respectively. Therefore, at high Pe_ω, where collision activated out-of-cage particle rearrangements are dominant, $\gamma_0 G_1'' \simeq \sigma(\dot{\gamma}_{\max})$, a measure of energy dissipation per unit strain, is proportional to shear rate ($\gamma_0\omega$) similar to the limiting high shear rate viscosity behavior under steady shear. On the other hand, at low Pe_ω, a $G_1'' \propto \gamma_0^{-1}$ dependence corresponds to a steady shear thinning response of a HS glass at the yield stress plateau with $\eta_{\mathrm{eff}} \propto \dot{\gamma}^{-1}$.

We should note that the absence of hydrodynamic interactions (HI) in the BD simulations do not appear to introduce some qualitative difference as compared to experiments for the range of Pe_ω studied here (up to about

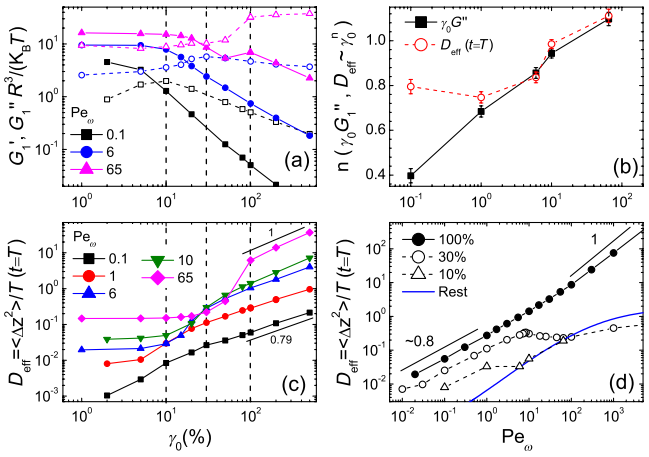

FIG. 4 (color online). BD simulations at $\varphi = 0.60$: (a) DSS data showing G_1' and G_1'' as a function of γ_0 for different Pe_ω as indicated. (b) Power law exponent for the γ_0 dependence of G_1'' and $D_{\mathrm{eff}}(t = T)$ as a function of Pe_ω. (c) Average $D_{\mathrm{eff}}(t = T)$ versus γ_0 for different Pe_ω, and (d) $D_{\mathrm{eff}}(t = T)$ versus Pe_ω for $\gamma_0 = 10\%$, 30%, and 100%. The corresponding $D_{\mathrm{eff}}(t = T)$ for a system at rest is also indicated.

100) as suggested by the similarity in the Lissajous plots (Fig. 2) and dynamic strain sweeps [Figs. 1 and 4(a)]. Along this line, the absence of a double G_1'' peak in BD cannot be attributed to the absence of hydrodynamic interactions, since BD at high volume fractions could not be conducted at a similar number of data points as experiments due to computational time restrictions. Nevertheless, a future direct comparison with Stokesian dynamics simulations (with full HI) would be quite valuable to pin-point details in the role of HI for $\mathrm{Pe}_\omega > 1$.

Further insight into the two yielding mechanisms is gained by examining microscopic particle dynamics within a LAOS cycle by BD. In Fig. 4(c), we show the effective diffusivity, $D_{\mathrm{eff}}(t = T) = \langle \Delta z^2(T) \rangle / T$ with $\langle \Delta z^2(T) \rangle$ the mean square displacement in the vorticity direction, z, (at $t = T$), as a function of γ_0 for several Pe_ω. At low Pe_ω, $D_{\mathrm{eff}}(T)$ increases sublinearly with γ_0, whereas as Pe_ω is increased it exhibits progressively a weaker increase at small γ_0 and a stronger one at higher γ_0. The constant $D_{\mathrm{eff}}(T)$ for $\gamma_0 \ll \gamma_y$ indicates that prior to yielding, in-cage diffusion is unaffected by shear; for the lowest Pe_ω, this regime is not reached since γ_y increases with frequency [9]. For $\gamma_0 > \gamma_y$, $D_{\mathrm{eff}}(T)$, corresponding to out-of cage diffusion, increases sublinearly [$\gamma_0 = 100\%$, Fig. 4(d)] with a power law exponent $\simeq 0.8$ at low Pe_ω, which approaches 1 for $\mathrm{Pe}_\omega > 1$ where direct particle collisions are dominant. In comparison, the corresponding $D_{\mathrm{eff}}(T)$ for $\gamma_0 = 10\%$ and 30% show an initial sublinear dependence at low Pe_ω and subsequently approach the curve at rest, since for such frequencies $\gamma_y > 30\%$ [9] and the sample has not yet yielded. Note that a similar power law increase (with exponent ~ 0.8) has been detected in HS glasses at low steady shear rates by confocal microscopy [6], a weak but systematic deviation from the linear MCT prediction [25] and closer to agreement with nonlinear Langevin equation theory involving activated hopping mechanisms [26]. For our oscillatory BD, a linear dependence is reached for $\mathrm{Pe}_\omega > 10$ as expected for non-Brownian particles under steady shear [27]. We suggest that the sublinear and linear dependencies probed here at low and high Pe_ω, respectively, reflect the two different mechanisms involved in the two regimes. Note that similarly with D_{eff}, $\gamma_0 G_1''$ increases linearly with γ_0 at high Pe_ω; the linear γ_0 dependence of both quantities is linked to collision-induced yielding. On the other hand, at low Pe_ω both quantities increase sublinearly, $D_{\mathrm{eff}} \propto \gamma_0^{0.8}$ and $\gamma_0 G_1'' \propto \gamma_0^{0.4}$ (the latter exponent tends to zero as Pe_ω is lowered) reflecting plastic flow, with a power law stress behavior, and complex Brownian motion and shear-activated particle hopping.

In summary, the combination of experimental oscillatory rheology and BD simulations has revealed the complete mechanical fingerprint of HS glasses and the related underlying microscopic structure and dynamics over a wide frequency regime where both Brownian and non-Brownian behavior is probed. At low Pe_ω, commonly studied up to now, Brownian-assisted irreversible motion takes place during yielding with a single peak of G_1'' and strong higher harmonics of the stress at large γ_0. In this regime, the microstructure under shear is only weakly anisotropic while the shear-induced diffusivity scales sublinearly with Pe_ω. At high Pe_ω, yielding is dictated by collision-induced displacements linked with a shear-induced long time diffusion that increases linearly with Pe_ω. A single G_1'' peak is detected at $\gamma_0 > \gamma_y$ which eventually turns into a plateau at the limit of large Pe_ω. The structure under shear is strongly anisotropic, but more interestingly, exhibits a hysteresis under strain reversal. Such structural memory, due to lack of Brownian relaxation, causes a characteristic stress drop after strain reversal as revealed by the Lissajous curves. At some characteristic γ_0, higher harmonics drop to almost zero indicating an unexpected harmonic response even though the sample is under nonlinear shear. Finally, at a φ dependent intermediate Pe_ω regime, the sample is affected by both mechanisms (Brownian- and collision-induced yielding) resulting in a double peak of G_1'' and two minima of higher harmonics, a feature that is detected for the first time in simple hard sphere glasses.

The rich mechanical response of a model hard sphere glass revealed in LAOS as a function of frequency, bridging the Brownian and non-Brownian regimes, may provide insights for the understanding of systems with more complicated interparticle interactions. These include both soft particle glasses that have been currently attracting significant interest (see, for example, Ref. [19]) as well as other pastes, slurries, particle gels, jammed emulsions, and metallic glasses.

We thank A. B. Schofield for the particles and acknowledge funding from EU FP7-Infrastructures 'ESMI' (CP&CSA-2010-262348) and Greek "Thales" Project "COVISCO".

*Corresponding author.
georgp@iesl.forth.gr

[1] J. Mewis and N. J. Wagner, *Colloidal Suspension Rheology*, Cambridge Series in Chemical Engineering (Cambridge University Press, New York, 2012).
[2] R. G. Larson, *The Structure and Rheology of Complex Fluids* (Oxford University Press, Oxford, 1999).
[3] P. Pusey and W. van Megen, Nature (London) **320**, 340 (1986).
[4] P. Pusey, in *Liquids, Freezing and Glass Transition: Proceedings Les Houches Summer School, 1989*, edited by J. P. Hansen, D. Levesque, and J. Zinn-Justin (Elsevier, Amsterdam, 1991).
[5] G. Petekidis, D. Vlassopoulos, and P. N. Pusey, J. Phys. Condens. Matter **16**, S3955 (2004).
[6] R. Besseling, E. R. Weeks, A. B. Schofield, and W. C. K. Poon, Phys. Rev. Lett. **99**, 028301 (2007).
[7] N. Koumakis, M. Laurati, S. U. Egelhaaf, J. F. Brady, and G. Petekidis, Phys. Rev. Lett. **108**, 098303 (2012).
[8] G. Petekidis, A. Moussaid, and P. N. Pusey, Phys. Rev. E **66**, 051402 (2002).
[9] G. Petekidis, D. Vlassopoulos, and P. Pusey, Faraday Discuss. Chem. Soc. **123**, 287 (2003).
[10] K. Hyun, M. Wilhelm, C. O. Klein, K. S. Cho, J. G. Nam, K. H. Ahn, S. J. Lee, R. H. Ewoldt, and G. H. McKinley, Prog. Polym. Sci. **36**, 1697 (2011).
[11] T. G. Mason and D. A. Weitz, Phys. Rev. Lett. **75**, 2770 (1995).
[12] J. M. Brader, M. Siebenbuerger, M. Ballauff, K. Reinheimer, M. Wilhelm, S. J. Frey, F. Weysser, and M. Fuchs, Phys. Rev. E **82**, 061401 (2010).
[13] P. Sollich, Phys. Rev. E **58**, 738 (1998).
[14] D. Pine, J. Gollub, J. Brady, and A. Leshansky, Nature (London) **438**, 997 (2005).
[15] P. Ballesta, R. Besseling, L. Isa, G. Petekidis, and W. Poon, Phys. Rev. Lett. **101**, 258301 (2008).
[16] R. Besseling, L. Isa, P. Ballesta, G. Petekidis, M. E. Cates, and W. C. K. Poon, Phys. Rev. Lett. **105**, 268301 (2010).
[17] C. Lopez-Barron, L. Porcar, A. Eberle, and N. Wagner, Phys. Rev. Lett. **108**, 258301 (2012).
[18] M. P. Lettinga, P. Holmqvist, P. Ballesta, S. Rogers, D. Kleshchanok, and B. Struth, Phys. Rev. Lett. **109**, 246001 (2012).
[19] N. Koumakis, A. Pamvouxoglou, A. S. Poulos, and G. Petekidis, Soft Matter **8**, 4271 (2012).
[20] See Supplemental Material at http://link.aps.org/supplemental/10.1103/PhysRevLett.110.178301 for description of BD simulations and movie of stresses and structures within LAOS.
[21] D. R. Foss and J. F. Brady, J. Rheol. **44**, 629 (2000).
[22] K. N. Pham, G. Petekidis, D. Vlassopoulos, S. U. Egelhaaf, W. C. K. Poon, and P. N. Pusey, J. Rheol. **52**, 649 (2008).
[23] N. Koumakis and G. Petekidis, Soft Matter **7**, 2456 (2011).
[24] K. Miyazaki, H. M. Wyss, D. A. Weitz, and D. R. Reichman, Europhys. Lett. **75**, 915 (2006).
[25] M. Fuchs and M. E. Cates, J. Rheol. **53**, 957 (2009).
[26] E. Saltzman, K. Yatsenko, and G. Schweizer, J. Phys. Condens. Matter **20**, 244129 (2008).
[27] A. Sierou and J. F. Brady, J. Fluid Mech. **506**, 285 (2004).